4-1-2019

The sp^2-sp^3 Carbon Hybridization Content of Nanocrystalline Graphite from Pyrolyzed Vegetable Oil, Comparison of Electrochemistry and Physical Properties with Other Carbon Forms and Allotropes

David Estrada
Boise State University

Paul H. Davis
Boise State University

Twinkle Pandhi
Boise State University

Katie Yocham
Boise State University

Kari Higginbotham
Boise State University

Publication Information

Estrada, David; Davis, Paul H.; Pandhi, Twinkle; Yocham, Katie; and Higginbotham, Kari. (2019). "The sp2-sp3 Carbon Hybridization Content of Nanocrystalline Graphite from Pyrolyzed Vegetable Oil, Comparison of Electrochemistry and Physical Properties with Other Carbon Forms and Allotropes". *Carbon, 144*, 831-840. http://dx.doi.org/10.1016/j.carbon.2018.12.058

The sp^2-sp^3 Carbon Hybridization Content of Nanocrystalline Graphite from Pyrolyzed Vegetable Oil, Comparison of Electrochemistry and Physical Properties with Other Carbon Forms and Allotropes.

Humayun Kabir[1], Haoyu Zhu[1], Jeremy May[1], Kailash Hamal[1], Yuwei Kan[1], Thomas Williams[2], Elena Echeverria[3], David N. McIlroy[3], David Estrada[4], Paul H. Davis[4], Twinkle Pandhi[4], Katie Yocham[4], Kari Higginbotham[4], Abraham Clearfield[5], I. Francis Cheng[1,*]

[1] Department of Chemistry, University of Idaho, 875 Perimeter Dr, MS 2343, Moscow, ID 83844, USA

[2] Department of Geological Sciences, University of Idaho, 875 Perimeter Dr, MS 3022, Moscow, ID 83844, USA

[3] Department of Physics, Oklahoma State University, 145 Physical Sciences Building, Stillwater, OK 74028, USA

[4] Micron School of Materials Science and Engineering, Boise State University, 1910 University Drive, Boise, ID 83725, USA

[5] Department of Chemistry, Texas A&M University, College Station, TX 77843, USA

*Corresponding author: Tel: (208) 885-6387, E-mail: ifcheng@uidaho.edu (I. Francis Cheng)

Abstract

Nanocrystalline (nc) graphite produced from pyrolyzed vegetable oil has properties that deviate from typical graphites, but is similar to the previously reported Graphite from the University of Idaho Thermolyzed Asphalt Reaction (GUITAR). These properties include (i) fast heterogeneous electron transfer (HET) at its basal plane and (ii) corrosion resistance beyond graphitic materials. To discover the structural basis for these properties, characterization of this nc-graphite was investigated with Raman and X-ray photoelectron spectroscopies, nano-indentation, density, X-ray diffraction (XRD), thermogravimetric and elemental analyses. The results indicate that this nc-graphite is in Stage-2 of Ferrari's amorphization trajectory between amorphous carbon (a-C) and graphite with a sp^2/sp^3 carbon ratio of 85/15. The nano-crystallites size of 1.5 nm from XRD is consistent with fast HET rates as this increases the density of electronic states at the Fermi-level. However, d-spacing from XRD is 0.350 nm vs. 0.335 for graphite. This wider distance does not explain its corrosion resistance. Literature trends suggest that increasing sp^2 content in a-C's increase both HET and corrosion rates. While nc-graphite's HET rate follows this trend, it exhibits higher than predicted corrosion resistance. In general, this form of nc-graphite matches the best examples of boron-doped diamond in HET and corrosion rates.

1. Introduction

Carbon electrodes offer the promise of low cost and high performance relative to other materials. The element itself is capable of forming many types of allotropes, each with a unique set of physicochemical properties. In electrochemical applications, the aqueous potential window and heterogeneous electron transfer (HET) kinetics with dissolved redox species are important from the standpoint of sensors and with electrochemical energy conversion and storage. [1,2,3,4] At the anodic potential limits, corrosion processes and water oxidation predominate (Reactions 1a and 1b).

$C + 2H_2O \rightarrow CO_2 + 4H^+ + 4e^-$ $E^0_{red} = 0.207$ V (1a)

$2H_2O \rightarrow O_2 + 4H^+ + 4e^-$ $E^0_{red} = 1.23$ V (1b)

On the other hand, at the cathodic potential limits, H_2 (g) evolution comes into consideration (Reaction 1c).

$2H^+ + 2e^- \rightarrow H_2$ $E^0_{red} = 0.00$ V (1c)

Slow electrode kinetics for the reactions above can increase effective stability up to a 2 V potential window on most graphitic electrodes. [5,6] In general, sp^3-C containing boron-doped diamond (BDD) and amorphous carbon (a-C) electrodes offer greater stability to corrosion than pure sp^2 carbon materials. [7,8,9,10] The sp^2/sp^3 ratio governs the chemical and physical characteristics of the carbon electrodes. In general, literature results suggest that increasing the sp^2 content will increase both rates of corrosion and HET kinetics. [5,6,7] The hybridization content (sp^2/sp^3 ratio) would also be important in determining atomic arrangement. Graphitic stacking would be expected of pure sp^2 materials, while structures with no layering would result from pure sp^3 materials. Most micrographs indicate that with mixed sp^2-sp^3 a-C materials do not exhibit layered morphology. [11,12,13,14,15] However, in a computational study, Galli and

coworkers examined an a-C consisting of 85% sp^2 and 15% sp^3, and predicted that the C atoms would form into a layered material.[16] The simulation also indicated that this a-C will have an increased density of electronic states at the Fermi level relative to crystalline graphite, which is expected to increase HET rates. [16,17]

The previously reported material, graphite (or graphene) from the University of Idaho Thermolyzed Asphalt Reaction (GUITAR) was initially mistaken for a graphite, as it has some physical and morphological similarities with sp^2-hybridized carbon materials. [18,19] Those initial characterizations best described this material as nanocrystalline (nc) graphite. In the search for increasing yields and scalability, the precursors for this material has varied. In this contribution, we examined a nc-graphite produced from pyrolyzed vegetable oil rather than the previously reported precursors. However, given that this material exhibits identical electrochemical, Raman spectroscopic, and x-ray diffraction characteristics as the previous GUITAR materials from this group, it will be referred to from this point on as GUITAR. [18,19,20,21]

Due to the combination of GUITAR's resistance to corrosion and fast HET rates, several investigations are underway examining applications in ultracapacitors, fuel cells, batteries and sensors. [4,20,21] In order to understand the stark differences in electrochemical characteristics between graphite and GUITAR, cyclic voltammetry, X-ray photoelectron spectroscopy (XPS), X-ray diffraction (XRD), and Raman studies were conducted to assess the sp^2/sp^3 carbon content and d-spacing of GUITAR with the goal of determining both shared and distinct structural characteristics with other forms of carbon. Density measurements, elemental, thermogravimetric (TGA), and hardness analyses were conducted to augment those studies. These measurements allow the placement of GUITAR in the sp^2-sp^3 carbon-H ternary phase diagram so that its

electrochemical characteristics be compared to the carbons of similar compositions. Quantitative measurements of corrosion were conducted by Tafel studies to ascertain any correlation with sp^3 content, and for comparison with anodically stable carbon electrodes with similar sp^2/sp^3 ratios.

2. Experimental

2.1 Chemicals

Deposition targets were constructed from quartz tubes (Technical Glass Products, Inc., Painesville Twp., OH, USA) cut into 2 cm x 0.5 cm wafers. The precursor for GUITAR deposition was vegetable (soybean) oil obtained from WinCo Foods grocery store in Moscow, Idaho, USA. The tube furnace was a Hevi Duty Electric Co., type M-3024. The peristaltic pump, steel injection needle, tubing, and thermocouple were acquired from McMaster-Carr (IL, USA). Nitrogen gas (>99.5 %) was supplied from Oxarc (WA, USA). Paraffin wax and high vacuum grease were obtained from Royal Oak Enterprises (GA, USA) and Dow Corning (MI, USA) respectively. Pyrolytic graphite foil (Lot # 157161) and graphite felt (KFD 2.5 EA) were obtained as gift from SGL Carbon Company (PA, USA). Highly ordered pyrolytic graphite (HOPG, ZYA) was obtained from SPI Supplies (PA, USA), with a mean step density 0.5±0.1 $\mu m/\mu m^2$, as reported by Unwin et al. [22] Sulfuric acid (96.3%) was purchased from J.T. Baker (NJ, USA). All aqueous stock solutions were prepared with deionized water, which was further purified by passage through an activated carbon purification cartridge (Barnstead, model D8922, Dubuque, IA).

2.2 GUITAR Synthesis from Vegetable Oil and Electrode Preparation

GUITAR samples were prepared via a chemical vapor deposition (CVD) method with the apparatus shown in Figure 1. This revised method obviates the need for sulfur as required in

previous studies. [18,19,23] The tube furnace was heated to a temperature of 900 ^{o}C and the carrier gas (N_2) purifier was preheated to 400 ^{o}C in a gas chromatograph gas purifier oven (Supelco, PA, USA). The deposition targets (2 cm x 0.5 cm, quartz slides) were positioned inside the quartz tube and the end was plugged with a small exhaust tube wrapped in ceramic wool to prevent O_2 from entering the chamber. The system was purged with preheated N_2 at a flow rate of 4.2 L/minute for 5 min prior to the start of run. Vegetable oil precursor was injected into the tube furnace at a rate of 5 mL/min for a total deposition time of 30 min. The tube furnace was then allowed to cool down under N_2 before the GUITAR coated substrates were removed.

Preparation of GUITAR working electrodes is described in previous publications [18,23]. GUITAR coated quartz slides were waxed leaving an exposed basal plane area of 0.1-0.2 cm^2. The graphite foil working electrodes were prepared by the same method.

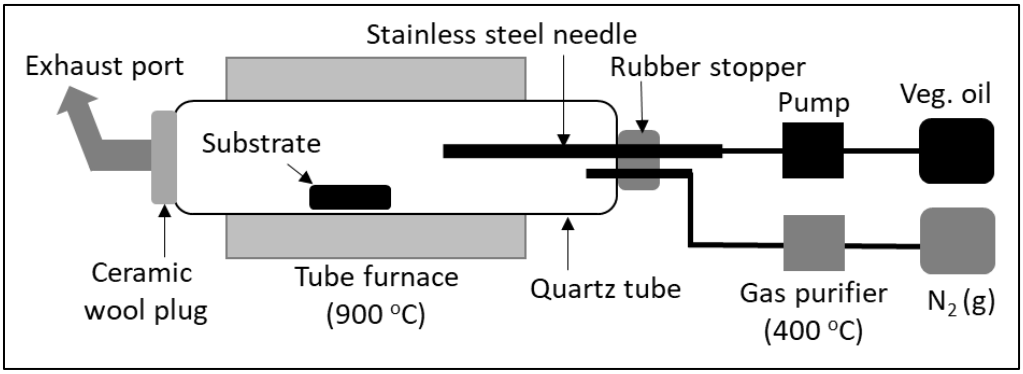

Figure 1. Schematic of GUITAR synthesis via chemical vapor deposition (CVD) method.

2.3 Characterization of GUITAR

Scanning electron microscope (SEM) images were obtained with a Zeiss Supra 35 SEM (Carl Zeiss, Germany). Density analyses were conducted by Micromeritics Particle Testing Authority (Norcross, GA, USA). Midwest Microlab (Indianapolis, IN, USA) did the elemental analysis for C, H, N and O. The XPS apparatus was built in-house at Oklahoma State University and performed in a vacuum chamber with a base pressure of 1×10^{-10} Torr. Measurements were

made with the Al Kα emission line (1486.6 eV) and a hemispherical energy analyzer with a resolution of 0.025 eV. All spectra were acquired at room temperature. The XPS peaks were fit with a Gaussian curve after performing a Shirley background subtraction. The FWHM were held at a constant value for all peaks. Raman spectrum was acquired with a Horiba LabRAM HR Evolution Raman microscope (Irvine, California) using a laser excitation wavelength of 514.5 nm. Hardness values were measured using a Hysitron TS 75 TriboScope nanoindenter head mounted on a Bruker Dimension 3100 AFM. A diamond tip Berkovich probe (Hysitron TI-0039) with a 100 nm nominal radius of curvature was used to create the indents. A series of indentations were carried out at loads varying from 0.3-25 mN.

Thermogravimetric analyses (TGA, Perkin Elmer TGA-7, Waltham, MA, USA) were conducted under air atmosphere (21 standard cubic centimeters per minute, or SCCM, flow rate) from ambient temperature to 900 °C with a heating rate of 10 °C/min. Samples used in TGA consisted of 1-2 mg of particles with a size <1 mm. Powder X-ray diffraction (XRD) was conducted on a Siemens D5000 Diffractometer (Germany) equipped with an FK 60-04 air insulated XRD tube and a Cu anode. The spectra were taken with Cu K-alpha radiation (0.154 nm) at 40 kV and 30 mA in the range of $2\theta = 0\text{-}80°$ at room temperature. Electrochemical measurements were carried out at room temperature using a Gamry PCI4/750 potentiostat (Gamry Instruments, Warminster, PA, USA). The reference electrode was an Ag/AgCl/3 M NaCl system (0.209 V vs. SHE). A KFD graphite felt (15 cm x 10 cm) served as the counter electrode. Tafel polarization measurements were carried out in N_2 saturated 1.0 M H_2SO_4 using a single compartment 1.0 L volume cell. The working electrodes were allowed to equilibrate in electrolyte solutions for ≥ 1 hour to attain an equilibrium or open circuit potential (E_{ocp}) prior to the start of polarization. The working electrodes were scanned from -0.5 to +1.0 V vs. Ag/AgCl

at a scan rate of 1 mV/s. These experiments were performed under vigorously stirred conditions. The standard HET rate constants (k^0, cm/s) for $Fe(CN)_6^{3-/4-}$ on GUITAR and other carbon electrodes were calculated using the Nicholson method as described in reference 24, and also determined by modeling with DigiSim version 3.03b (Bioanalytical Systems, Inc. West Lafayette, IN, USA). The k^0 values obtained from modeling agreed with the Nicholson method. Above a cyclic voltammetric potential peak separation (ΔE_p) greater than 212 mV, only DigiSim was used for the determination of k^0 for literature carbon materials, as Nicholson's analysis is limited to ΔE_p 212 mV. The transfer coefficient (α) and diffusion coefficient (D) for $Fe(CN)_6^{3-/4-}$ are assumed as 0.5 and 6×10^{-6} cm^2/s respectively, as reported in literature. [25,26,27]

3. Results and Discussion

3.1 Micrographs of the *nc-Graphite, GUITAR and Highly Ordered Pyrolytic Graphite (HOPG)*

Optical and scanning electron micrographs show GUITAR has clearly discernable basal and edge planes with a layered structure, similar to previous synthetic methods and to graphites and graphenes. [18,19] Figure 2 illustrates these configurations and similarities between GUITAR and highly ordered pyrolytic graphites (HOPG). However, an important feature observed with graphites is missing with GUITAR as its basal plane is flat and featureless to the resolution of SEM. On the other hand, the basal plane of HOPG exhibits its characteristic step defects. The mean step density of the HOPG (ZYA) is calculated as 0.5±0.2 $\mu m/\mu m^2$ using SEM images. This value agrees with the result reported by Unwin et al. (0.5±0.1 $\mu m/\mu m^2$, using atomic force microscopy). [22] More SEM images are presented in the supplementary information contrasting the edge and basal planes of GUITAR and HOPG (see Figure S1). No step defects have been

observed on the basal plane of GUITAR in over 200 SEM images over several years (2010-2018).

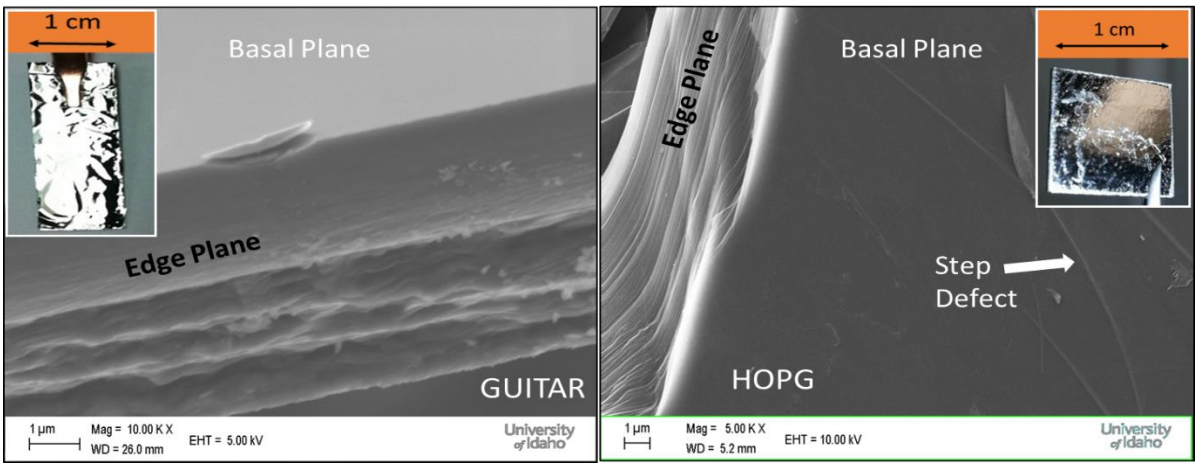

Figure 2. Photographs (insets) and scanning electron micrographs illustrating morphological similarities between GUITAR and highly ordered pyrolytic graphite (HOPG). Both show clear basal and edge plane configurations.

3.2 Electrochemical Properties of GUITAR

Despite the morphological similarities, GUITAR has electrochemical properties that diverge from graphites and graphenes. These include fast HET rate across its basal plane (BP) and resistance to corrosion as measured by cyclic voltammetry. The results obtained with the newest and simplified synthetic process of this contribution are in concordance with previous studies. [19,20,21,28] The $Fe(CN)_6^{3-/4-}$ redox probe is often employed to measure these rates on carbon materials (Reaction 2). [29,30,31]

$$Fe(CN)_6^{3-} + e^- \rightleftharpoons Fe(CN)_6^{4-} \qquad E^0_{red} = 0.430\ V \qquad (2)$$

Cyclic voltammetric experiments were conducted on GUITAR electrode with 1 mM $Fe(CN)_6^{3-}$ in 1 M KCl at 50 mV/s with a measured ΔEp of 65 mV. This replicates previous studies of GUITAR with various synthetic methods. [19,20,21] That ΔEp corresponds to a standard rate constant (k^0) of 0.03 cm/s as calculated from the Nicholson method as well as determination by

modelling with DigiSim software. This exceeds the basal planes of other graphites and graphenes by 2-6 orders of magnitude [19,29,32,33]. Slow kinetics on the BP of crystalline graphites is attributed to the low density of electronic states (DOS) at the Fermi-level. [29,30] On the other hand, the defect-rich nanocrystallinity of GUITAR would increase that DOS. [19,30] The measured 200 μA/cm^2 anodic limit of 1.9 V vs. Ag/AgCl in 1.0 M H_2SO_4 at 50 mV/s matches previous studies. [19,20] This is 300 to 500 mV greater than graphites in various electrolytes. [5,6,19,20] This resistance to corrosion is attributed to the lack of electrolyte intercalation through the edge and basal planes of GUITAR as discussed in previous studies. [19] The total potential window at 200 μA/cm^2 in 1 M H_2SO_4 is 3 V, which surpasses graphites by 1 V. [19,20,21] Both the CV of $Fe(CN)_6^{3-/4-}$ and the potential windows are shown in Figure S2 of the supplementary information.

3.3 Density of GUITAR is Consistent with Graphites and Amorphous Carbons

Skeletal and bulk densities of GUITAR were measured as 1.95 and 0.57 g/cm^3 respectively. This is consistent with literature graphites that have skeletal and bulk densities of 1.6-2.3 g/cm^3 and 0.22-0.59 g/cm^3 respectively. [34,35,36] It is also similar to the skeletal densities of a-C and hydrogenated amorphous carbons (a-C:H) which range between 1.6-2.2 and 1.2-2.4 g/cm^3 respectively. [35,36,37,38] The skeletal density of GUITAR lies well below that of diamond (3.51 g/cm^3) and DLC (2.35-3.26 g/cm^3), but above that of glassy carbon (1.3-1.5 g/cm^3). [36,39,40] Also of interest is the agreement of the skeletal density for GUITAR with the computational value for an a-C consisting of 15% sp^3-C reported by McKenzie (see Figure 21 therein). [41] Based on density, GUITAR can be placed in the range expected of graphitic to a-C materials.

3.4 Elemental Analysis Indicates GUITAR is a Hydrogenated Carbon Material

The results of this study yield 98.72% C, 0.20% O and 1.08% H by mass (88.35% C, 0.14% O and 11.51% H by mole) for GUITAR. This matches results obtained with XPS analysis below. It is noteworthy that GUITAR is one of the purest carbon films grown by a CVD method, and significantly, shows no metal contamination and negligible oxygen content. Literature CVD-grown graphenes typically contain metal contamination and 5-30 wt% oxygen. [42,43,44] Furthermore, elemental analysis indicates that GUITAR possesses more hydrogen content that would be expected of most graphites but within the range of graphite-like hydrogenated a-C (GLCH, <20 atomic %). [45]

3.5 XPS Analysis Indicates that GUITAR is 15% sp^3-Carbon

Figure 3A shows the full scan XPS spectrum of GUITAR, where only the C1s peak is observed. This agrees with the results from elemental analysis. In Figure 3B the deconvolved C1s peak reveals 3 components: sp^2-C (284.2 eV) at 85.0% abundance, sp^3-C (285.4 eV) at 15.0%, and a satellite peak typical of sp^2 carbon at 286.9 eV. [46] The sp^2 content of GUITAR is close to, but slightly below that of literature graphites, which range from 90 to 100%. [47,48] In contrast, the sp^2 carbon content of a-C and DLC electrodes varies from 10-75%. [7,49,50,51] Another graphite-like material, turbostratic carbon consists of 70% sp^2 carbon. [52] This places GUITAR's sp^2 content midway between the lower bound of graphites and the upper end of a-C.

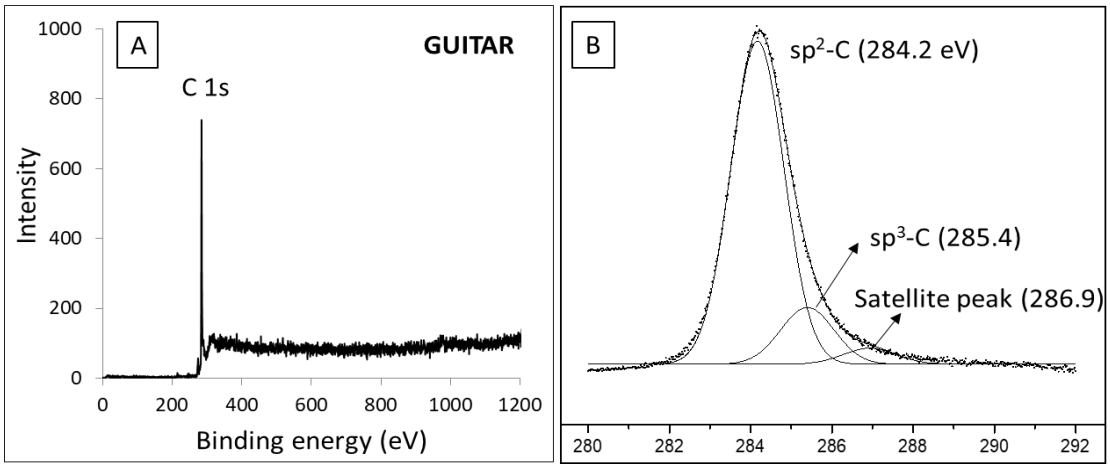

Figure 3. (A) Wide scan XPS spectra of GUITAR and (B) Deconvolved peaks of the C1s signal.

3.6 Raman Studies of GUITAR Indicate that it has Characteristics of Nanocrystalline Graphite and Graphite-Like Hydrogenated a-C

Figure 4 illustrates the Raman spectrum of GUITAR obtained with a laser excitation wavelength of 514.5 nm. In graphitic materials the G-band (1575-1600 cm^{-1}) is associated with the E_{2g} vibrational mode within the graphene lattice, while the D-band (1350-1380 cm^{-1}) is associated with a breathing mode that appears due to defects in that lattice. [53,54] For GUITAR, the ratio of the intensities, I(D)/I(G) = 1.16 with the D and G band positions at 1359 and 1591 cm^{-1} respectively. Using that data in the Raman analysis of Figure 5 in reference 45 yields a H atomic % of ~10% which is in good agreement with the elemental analysis of this study (11.51% H). In Figure 5 of reference 49, the G-band position of GUITAR (1591 cm^{-1}) is found to be intermediate to nano-crystalline graphite (nc-G, 1600 cm^{-1}) and graphite-like hydrogenated a-C (GLCH, 1560 cm^{-1} and 16% H).

A Raman spectrum of GLCH with 12% atomic H that could not be located in literature. GLCH with 16% H differs significantly from GUITAR with reported D and G band positions at

1385 and 1569 cm^{-1} respectively, and I(D)/I(G) = 0.60. [14] Another carbon material with exposed nc-graphene edges and an sp^2-C content of 85-87% has similar Raman and electrochemical characteristics (see Section 3.11) with GUITAR. [55] Ferrari's amorphization trajectory offers further insights based on the placement of carbon materials in one of three stages, (1) graphite to nanocrystalline graphite (nc-G, 100% sp^2), (2) nc-G to a-C (up to 20% sp^3) and (3) a-C to tetrahedral a-C (ta-C, up to 85% sp^3). Based on G-positions and I(D)/I(G) ratios, GUITAR is in Ferrari's Stage 2, near the transition with Stage 1. The reported GLCH with 16% H is again in Stage 2 but near the transition to Stage 3. [56,57] The full width at half maximum (FWHM) of the G-band in Figure 4 of 79 cm^{-1} gives an L_a (crystal grain size) of 2-5 nm based on an analysis by Ferrari and Robertson. [57] This is consistent with a previous investigation of GUITAR that gave an L_a of 1.5 nm and the XRD results below (see Section 3.10). [58 (manuscript submitted)]

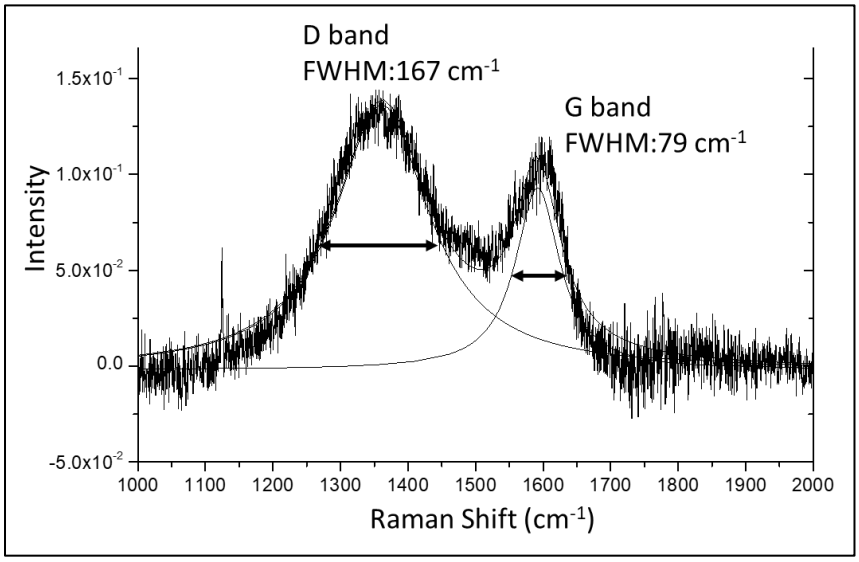

Figure 4. Raman spectrum of GUITAR at 514.5 nm laser excitation wavelength. The D and G bands peaks are at 1359 and 1591 cm^{-1} respectively with I(D)/I(G) intensity ratio of 1.16. The deconvolved peaks are shown with the FWHM of the D and G bands at 167 and 79 cm^{-1} respectively.

3.7 Hardness Analysis of GUITAR is Consistent with 15% sp^3-C Content

The hardness of carbon increases with increasing sp^3-C content with the transition from graphite to diamond covering 0 to 100 gigapascals (GPa). [59,60] For GUITAR the hardness is 5.6 ± 1 (n = 20) GPa as measured via nanoindentations. Figure 5 illustrates that GUITAR, with its 15% sp^3-C content as obtained by XPS, lies along the linear trend between 0-100% sp^3 when compared with other carbon materials in the literature. [14,59,60,61,62,63,64]

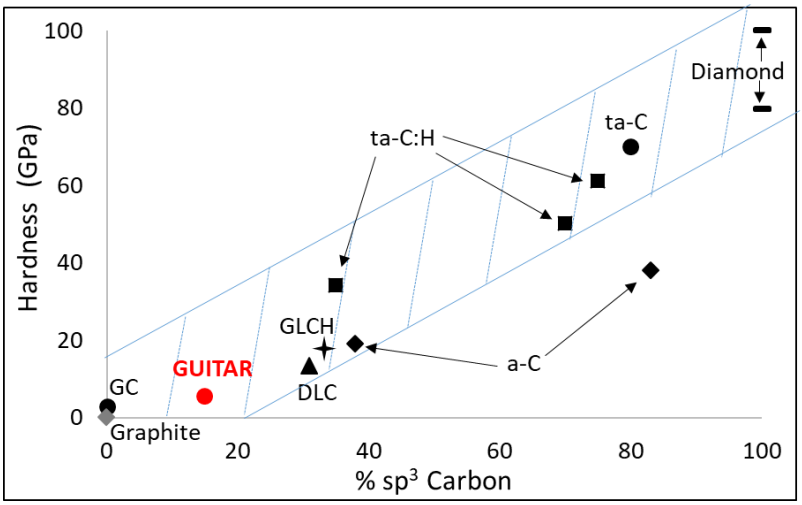

Figure 5. Hardness (GPa) vs. sp^3-C content for different carbon forms. Abbreviations: a-C = Amorphous Carbon, ta-C = Tetrahedral a-C, ta-C:H = Hydrogenated tetrahedral a-C. GLCH = Graphite like hydrogenated a-C, DLC = Diamond like Carbon, GC = Glassy Carbon.

3.8 Thermogravimetric analysis (TGA) of GUITAR Indicates a Graphite-like Homogeneous Mixture

From the analyses presented up to this point, GUITAR appears to be mostly graphitic in nature with some hydrogenated a-C content. Carbon materials with a heterogeneous mixture of graphitic and a-C exhibit two decomposition temperatures (T_d), one for each type of carbon. [65,66] To investigate this possibility in GUITAR, thermogravimetric analysis of both GUITAR and HOPG were conducted under flowing air, with the results shown in Figure 6. The T_d onsets

are 640 and 700 °C for GUITAR and HOPG powders respectively as determined by the first derivative method (Δm/ΔT). [67] The T_d of GUITAR conforms with literature graphites which range from 610-680 °C. [66,68,69] For comparison, the decomposition temperatures of other carbon materials are: 525-600 °C for BDD and 250-410 °C for both a-C and DLC. [65,70,71,72,73,74] Significantly, the single T_d of GUITAR indicates a homogeneous composition of graphite-like carbon, rather than a mixture that includes a-C.

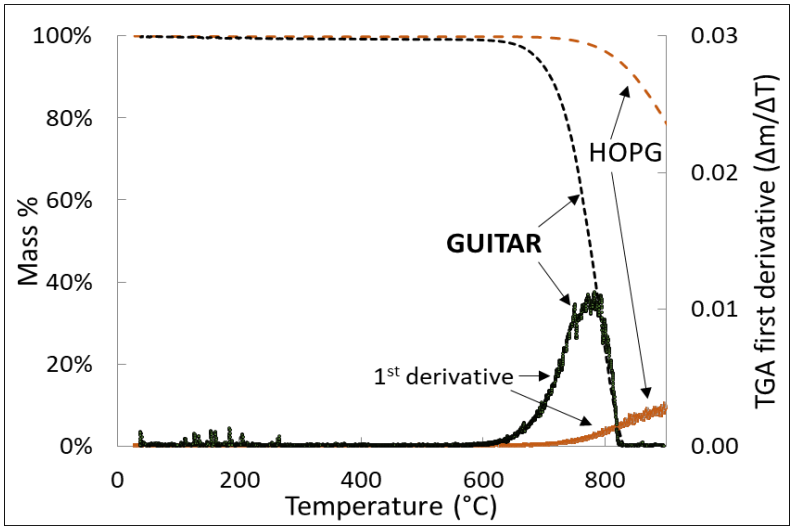

Figure 6. Thermogravimetric (TGA) curves of GUITAR and HOPG in the presence of air.

3.9 Placement of GUITAR in the sp^2-sp^3 Carbon-Hydrogen Phase Diagram is between Graphite and GLCH

Figure 7 illustrates the carbon ternary phase diagram. [45] Based on the analyses thus far, the position of GUITAR is in the border region of GLCH (graphite like hydrogenated amorphous carbon) using the Ferrari and coworkers classification system. These materials have less than 20

atomic % H with high sp^2-C content. [45] This placement is consistent with the Raman spectrum, indicating that GUITAR is intermediate between nc-graphite and GLCH.

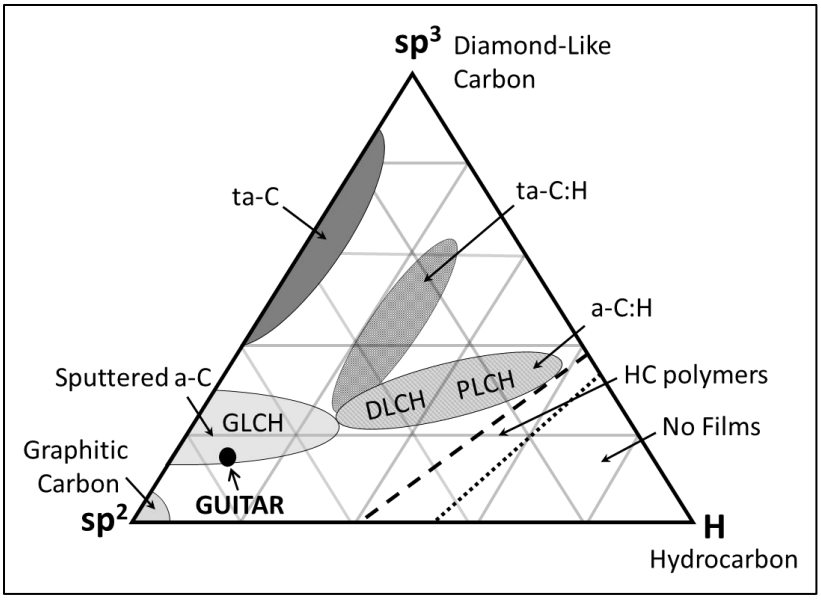

Figure 7. Placement of GUITAR (75.1% sp^2-C, 13.2% sp^3-C and 11.5% H by mole) in the sp^2-sp^3-H ternary phase diagram for carbon. Abbreviations: a-C = Amorphous Carbon, a-C:H = Hydrogenated a-C, ta-C = Tetrahedral a-C, ta-C:H = Tetrahedral a-C:H, GLCH = Graphite like a-C:H, DLCH = Diamond like a-C:H and PLCH = Polymer like a-C:H.

3.10 Measurement of Crystallite Grain Size (L_a) and d-spacing by X-ray Diffraction, Relationships with Fast HET Rates and Resistance to Corrosion

Crystalline graphites typically exhibit relatively slow $Fe(CN)_6^{3-/4-}$ HET kinetics, although some studies indicate an initial fast rate with degradation after a few hours. [33,75] Sluggish HET kinetics is attributed to the low density of electronic states (DOS) near the Fermi-level of graphite [29,30]. The DOS increases with disorder in the graphite lattice, which increases the HET rate. This feature is hypothesized to be the basis of the relatively fast HET rate observed for BP-GUITAR (k^0 = 0.03 cm/s). The standard rate constant (k^0) for $Fe(CN)_6^{3-/4-}$ on BP-GUITAR matches that of edge plane HOPG, while surpassing the kinetics of BP HOPG by 10^6 [29,32]. Furthermore, GUITAR maintains excellent stability for k^0 over 24 hours. [19] The crystal grain

size (L_a) for HOPG is 100-1000 nm with $k^0 \approx 10^{-6}$ to 10^{-9} cm/s. [19,33] Based on $Fe(CN)_6^{3-/4-}$ HET rates the L_a for GUITAR is expected to be much smaller.

Figure 8 shows the XRD spectra of GUITAR and HOPG. GUITAR exhibits a strong basal reflection (002) peak at $2\theta = 25.4°$ which is close to classical graphites ($2\theta = 26.5$-$27°$). [76,77] A previous Raman study of GUITAR indicated a nano-crystallite grain size (L_a) of ~1.5 nm. [58] This is in good agreement with X-ray diffraction-based estimates of $L_a = 1.6$ nm as calculated in this study from Scherrer's law ($L_a = (K\lambda)/(B \cos\theta)$, where K is the crystallite shape factor = 0.94, λ is the X-ray wavelength, B is the full width at half maximum of the peak, and θ the Bragg angle. [78] The XRD analysis was also used to obtain the d-spacing of GUITAR and the reference HOPG material.

Generally, wider d-spacing enhances electrolyte intercalation, the initial step leading to electrode corrosion. [79,80,81] However, the d-spacing in GUITAR is calculated as 0.350 nm from Bragg's Equations ($n\lambda = 2d \sin(\theta)$, with n = 1), while the reference HOPG gives 0.335 nm, in agreement with the literature. [82,83] It is apparent that GUITAR's d-spacing is wider than both graphites (0.335-0.340 nm) and glassy carbons (0.335-0.342 nm). [82,83,84,85] On multiwall carbon nanotubes (MWCNT) and onion-like carbons the d-spacing is 0.340-0.390 nm and 0.336 nm respectively. [86,87,88] GUITAR's d-spacing is most similar to turbostratic carbons (0.342-0.365 nm), coals (0.334-0.362 nm) and graphites with AA stacking (0.352-0.366 nm). [89,90,91,92,93,94] It is significant to note that micrographs of turbostratic carbon do not exhibit discernable layered structures as does GUITAR (Figure 2). [52] This increased d-spacing relative to graphites might be expected of nanocrystalline GUITAR as predicted by a computational analysis by Belenkov, which calculates increase of d-spacing from 0.338 to 0.352 nm as L_a decreases from infinity to 0.6 nm. [95]

As increased d-spacing is associated with more facile electrolyte intercalation, the measured d-spacing runs contra to previous cyclic voltammetric studies of GUITAR which indicated no such behavior (Figure 4 in Ref. 19). [19,79] Computational models of a-C with the same sp^3 carbon composition of 15% as GUITAR predict the formation of inter-planar bonds in a layered graphite-like morphology. [16,17] Thus a possible hypothesis is that decreased electrolyte intercalation is from inter-planar bonds that prevent this process from occurring, increasing the corrosion resistance of GUITAR relative to graphites. [19] Future investigations will examine this hypothesis.

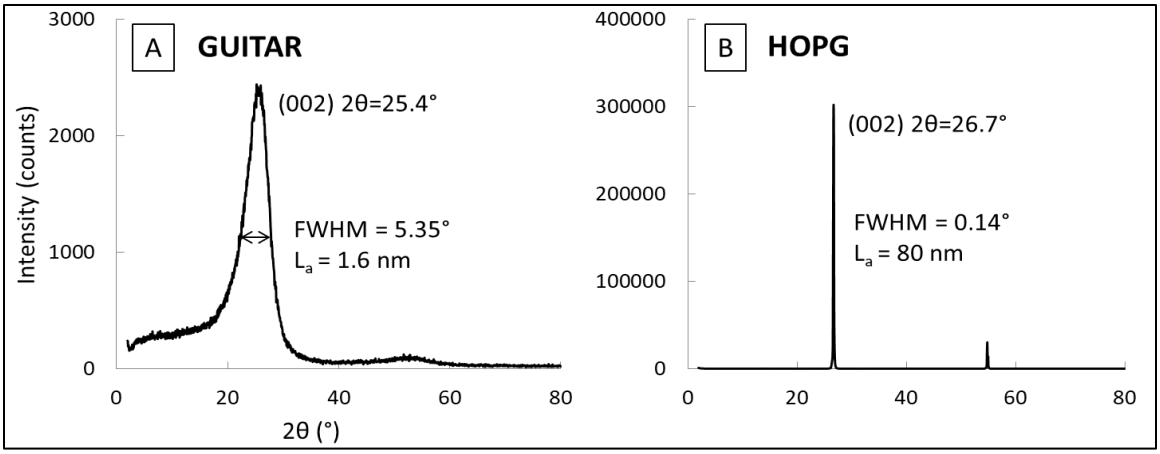

Figure 8. X-ray diffraction (XRD) analysis of (A) GUITAR and (B) Highly ordered pyrolytic graphite (HOPG).

3.11 The Role of Carbon Hybridization in the Corrosion of GUITAR: Tafel Studies

In contrast to graphene and graphites, the anodic potential limit of GUITAR is similar to materials containing sp^3-hybridized carbon. These include BDD, diamond-like carbons (DLC) which are primarily sp^3-C, and a-C which have various ratios of sp^2 and sp^3 carbons. [5,6,7,19,96,97,98,99,100] The sp^2/sp^3 ratio plays a strong role in the electrochemical behavior of a-C electrodes. [5,7,97] As discussed in the Introduction, as that ratio increases, the HET

kinetics for $Fe(CN)_6^{3-/4-}$ improve. On the other hand, increasing sp^2/sp^3 typically decreases resistance to corrosion. [5,7] The sp^2 content of GUITAR was established above as 85% by XPS. Relative to other anodically stable carbon materials, this is high and thus GUITAR would be expected to have lower resistance to corrosion relative to high sp^3 carbon materials, albeit with superior HET rates. Classical Tafel studies allow for the quantitative assessment of corrosion. Tafel studies were therefore conducted on GUITAR in 1.0 M H_2SO_4 using BP-pyrolytic graphite as a control, with the results shown in Figure 9.

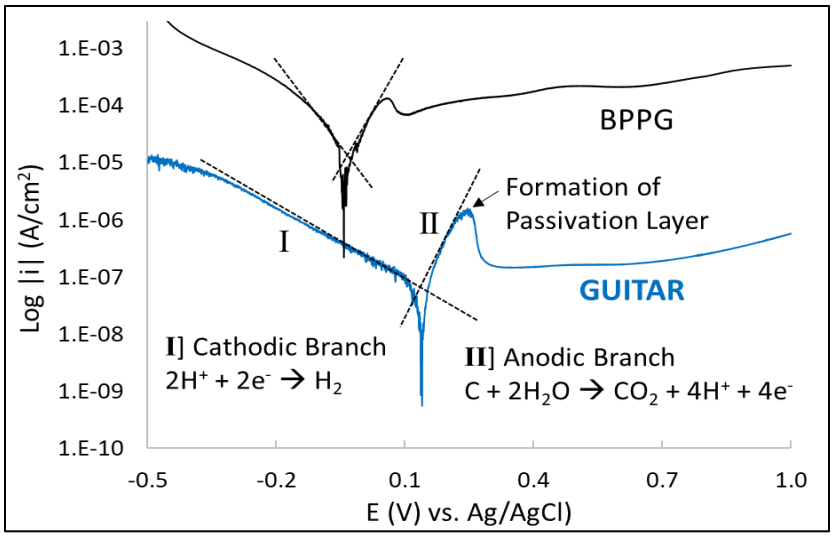

Figure 9. Tafel plots obtained at 1 mV/s for basal plane pyrolytic graphite (BPPG) and basal plane GUITAR in 1.0 M H_2SO_4. Extrapolation of Tafel plot to give i_{corr} and E_{corr} are shown along with the electrochemical reactions for the anodic and cathodic branches. Both BPPG and GUITAR exhibit the formation of a passivation layer.

Extrapolations of the Tafel plots for GUITAR in 1.0 M H_2SO_4 give an i_{corr} (corrosion current) of $2.4 \pm 1.5 \times 10^{-8}$ A/cm^2 and E_{corr} (corrosion potential) of 126 ± 15 mV vs. Ag/AgCl (both i_{corr} and E_{corr} are given as average ± standard deviation for 5 measurements). For comparison, the BPPG sample gave i_{corr} of 1.9×10^{-5} A/cm^2 and E_{corr} of -40 mV vs. Ag/AgCl respectively, these values are typical of graphite electrodes. [10,101,102] The rate of corrosion for GUITAR is three orders of magnitude lower than the pure sp^2 material. The passivation layers evident in the Tafel plots

for BPPG and GUITAR arise from the formation of oxide layers that inhibit electron transfer. These behaviors are typical for carbon electrodes. [10,101,102,103]

Figure 10A demonstrates the trend of corrosion rates increasing with sp^2 content for GUITAR and literature a-C and graphitic electrodes. [8,9,14,104,105,106,107,108]

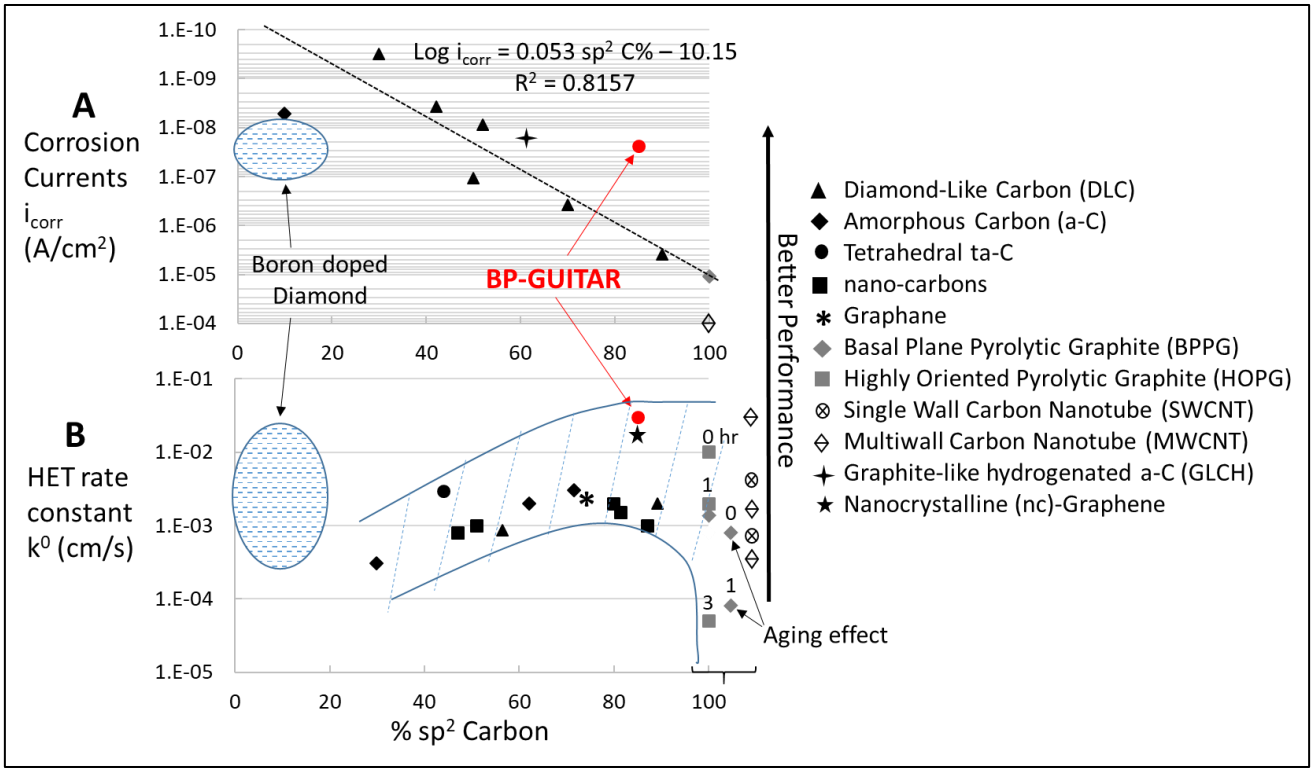

Figure 10. A) Corrosion currents (i_{corr}) vs. sp^2-C content for carbon electrodes. A linear trend for log (i_{corr}) vs % sp^2-C in amorphous carbon is noted. GUITAR is an outlier in that trend. B) HET rates for $Fe(CN)_6^{3-/4-}$ expressed as k^0 (cm/s). The outlined region is the observed trend for amorphous (30-85% sp^2) and graphitic (100% sp^2) carbons. HOPG and BPPG age over time in air or solution, which eventually lowers the HET rates.

A linear relationship between log i_{corr} and % sp^2-C is evident from the trend for amorphous and graphitic carbons. BDD (sp^3-C) electrodes do not conform to this trend. GUITAR is an outlier relative to that linear trend, exhibiting more resistance to corrosion than expected. Its deviation from that trend is about 1.5 orders lower than what would be predicted for an a-C of GLCH with

15% sp^3-C content. This is unexpected given its wider d-spacing (0.350 nm) relative to graphite (0.335 nm).

Figure 10B illustrates the trend between the extent of sp^2 hybridization and literature $Fe(CN)_6^{3-/4-}$ HET rates (k^0, cm/s), which reach a maximum at 85% sp^2-C. [5,6,25,31,98,55,108,109,110,111,112,113,114,115,116]. The literature values were obtained by Nicholson's method or DigiSim software as explained in the Experimental. [24] The BDD electrodes again fall outside the trends associated with the a-C to graphite series. The wide variation of the performance of the 100% sp^2-C material is based on aging effects that lower HET rates with exposure time to air or solution. [32] It is noteworthy that such effects are much less pronounced with the BP of GUITAR. [19] The MWCNT closest to the k^0 of BP-GUITAR (0.03 cm/s) is an edge plane material, and edge plane materials are known to exhibit faster HET rates compared to basal plane materials. [30,31] The nc-graphene electrode close to the k^0 of GUITAR also consists of ~85/15 sp^2/sp^3, in that case the investigators attribute that behavior to edge planes exposed to solution. [55] The investigators did not conduct Tafel i_{corr} analyses of their materials, but it is expected to match the performances of GUITAR based on their potential window of 3.2 V at 500 μA/cm^2 in 0.05 M H_2SO_4. Overall, in the literature search of this contribution, GUITAR maintains excellent performance matching BDD for its combination of excellent HET rate and high resistance to corrosion. Furthermore, it is expected that GUITAR will have lower production costs than many of the other carbon materials of Figure 10.

4. Conclusions

Relative to other methods of depositing a-C films, the method described in this contribution is significantly less expensive and simpler. It is expected that GUITAR will prove to be more

economically viable for large-scale implementation relative to BDD. The latter requires high cost substrates, while GUITAR utilizes an inexpensive starting material (vegetable oil) that can be deposited on a variety of common substrates, including carbon fiber and stainless steel. It produces a graphitic film referred to as GUITAR, which, based on density measurements, elemental analysis, XPS, Raman spectroscopy, hardness, TGA, and XRD, indicates that GUITAR is a material intermediate of nc-Graphite and GLCH. It maintains the layered configuration of graphite, a morphology not seen with other amorphous carbons, but predicted by a 1989 computational analysis of a material with the identical composition of GUITAR. [16] Significantly, that model predicts a higher DOS at the Fermi-level for this type of material than crystalline graphites, which may form the basis for the observed higher HET rates at its BP over graphites and graphenes. The XRD and a previous Raman analysis indicate that GUITAR has a grain size (L_a) of about 1.5 nm. This would increase the disorder within the BP and the DOS in GUITAR. Both the sp^2-C content of 85% and the wider d-spacing (0.350 nm) relative to graphites (0.335 nm), seem to run contra to the observed low rate of corrosion by Tafel analysis, which gave 2.4×10^{-8} A/cm^2. This is one of the lowest rates measured on any electrode material. An unexplored hypothesis is the formation of inter-planar bonds that would limit the intercalation of electrolytes, which is the nascent phase of corrosion. Compared to existing materials greater than 30% sp^2-C (a-C to graphite), GUITAR offers the highest performance in terms of both resistance to corrosion and HET kinetics, matching the best examples of BDD in performance, with added versatility and lower cost.

Acknowledgements

We acknowledge X-ray Diffraction Laboratory at Texas A&M University for the use of the PXRD facilities and an unrestricted gift from ABB Group that partially supported this research. D.E., T.P. and P.H.D acknowledge startup funding from the Micron School of Materials Science and Engineering. D.E. acknowledges career development support through Institutional Development Awards (IDeA) from the National Institute of General Medical Sciences of the National Institutes of Health under Grants #P20GM103408 and P20GM109095.

References

[1] Liangsheng Hu, Xiang Peng, Kaifu Huo, Rongsheng Chen, Jijiang Fu, Yong Li, Lawrence Y.S. Lee, Kwok Y. Wong, Paul K. Chu. Dominant Factors Governing the Electron Transfer Kinetics and Electrochemical Biosensing Properties of Carbon Nanofiber Arrays. ACS Applied Materials & Interfaces 2016, 8, 28872-28879.

[2] Shengli Chen, Yuwen Liu, Junxiang Chen. Heterogeneous electron transfer at nanoscopic electrodes: importance of electronic structures and electric double layers. Chemical Society Reviews 2014, 43, 5372-5386.

[3] P. Suvarnaphaet, S. Pechprasarn. Graphene-Based Materials for Biosensors: A Review. Sensors 2017, 17(10), 2161.

[4] H. Kabir, I.O. Gyan, I.F. Cheng. Electrochemical modification of a pyrolytic graphite sheet for improved negative electrode performance in the vanadium redox flow battery. Journal of Power Sources 2017, 342, 31-37.

[5] Y. Tanaka, M. Furuta, K. Kuriyama, R. Kuwabara, Y. Katsuki, T. Kondo, A. Fujishima, K. Honda. Electrochemical properties of N-doped hydrogenated amorphous carbon films fabricated by plasma-enhanced chemical vapor deposition methods. Electrochimica Acta 2011, 56(3), 1172-1181.

[6] H.B. Martin, A. Argoitia, U. Landau, A.B. Anderson, J.C. Angus. Hydrogen and oxygen evolution on Boron-Doped Diamond electrodes. Journal of the Electrochemical Society 1996, 143(6), L133-L136.

[7] K. Honda, H. Naragino, Y. Shimai. Control of Electric Conductivity and Electrochemical Activity of Hydrogenated Amorphous Carbon by Incorporating Boron Atoms. Journal of The Electrochemical Society 2014, 161(10), B207-B215.

[8] Renhui Zhang, Juan Zhao, Yingchang Yang. A novel diamond-like carbon film. Surfaces and Interfaces 2017, 7, 1-5.

[9] Renhui Zhang, Liping Wang, Wei Shi. Variable corrosion behavior of a thick amorphous carbon coating in NaCl solution. RSC Advances 2015, 5, 95750-95763.

[10] F. Beck, H. Krohn, E. Zimmer. Corrosion of graphite intercalation compounds. Electrochimica Acta 1986, 31(3), 371-376.

[11] C. Louro, C.W. Moura, N. Carvalho, M. Stueber, A. Cavaleiro. Thermal stability in oxidative and protective environments of a-C:H cap layer on a functional gradient coating. Diamond & Related Materials 2011, 20, 57-63.

[12] T. Frauenheim, G. Jungnickel, T. Kohler, U. Stephan. Structure and electronic properties of amorphous carbon: from semimetallic to insulating behaviour. Journal of Non-Crystalline Solids 2011, 182, 186-197.

[13] M.H. Kim, J.Y. Lee. Thermal analysis of hydrogenated amorphous carbon films prepared by plasma enhanced chemical vapour deposition. Journal of Materials Science 1991, 26, 4787-4794.

[14] T.M. Manhabosco, A.P.M. Barboza, R.J.C. Batista, B.R.A. Neves, I.L. Müller. Corrosion, wear and wear–corrosion behavior of graphite-like a-C:H films deposited on bare and nitrided titanium alloy. Diamond & Related Materials 2013, 31, 58-64.

[15] Meidong Huang, Xueqian Zhang, Peiling Ke, Aiying Wang. Graphite-like carbon films by high power impulse magnetron sputtering. Applied Surface Science 2013, 283, 321-326.

[16] Giulia Galli, Richard M. Martin, Roberto Car, Michele Parrinello. Structural and Electronic Properties of Amorphous Carbon. Physical Review Letter 1989, 62, 555-558.

[17] Giulia Galli, Richard M. Martin, Roberto Car, Michele Parrinello. Ab initio calculation of properties of carbon in the amorphous and liquid states. Physical Review B 1990, 42, 7470-7482.

[18] I.F. Cheng, Y.Q. Xie, R.A. Gonzales, P.R. Brejna, J.P. Sundararajan, B.A.F. Kengne, D.E. Aston, D.N. McIlroy, J.D. Foutch, P.R. Griffiths. Synthesis of graphene paper from pyrolyzed asphalt. Carbon 2011, 49(8), 2852-2861.

[19] I.O. Gyan, P.M. Wojcik, D.E. Aston, D.N. McIlroy, I.F. Cheng. A Study of the Electrochemical Properties of a New Graphitic Material: GUITAR, ChemElectroChem 2015, 2(5), 700-706.

[20] I.O. Gyan, I.F. Cheng. Electrochemical study of biologically relevant molecules at electrodes constructed from GUITAR, a new carbon allotrope. Microchemical Journal 2015, 122, 39-44.

[21] H. Kabir, I.O. Gyan, J.D. Foutch, H. Zhu, I.F. Cheng. Application of GUITAR on the negative electrode of the Vanadium redox flow battery: improved $V^{3+/2+}$ heterogeneous electron transfer with reduced hydrogen gassing. Journal of Carbon Research C 2016, 2(2), 13.

[22] A.N. Patel, M.G. Collignon, M.A. O'Connell, W.O.Y. Hung, K. McKelvey, J.V. Macpherson, P.R. Unwin. A New View of Electrochemistry at Highly Oriented Pyrolytic Graphite. Journal of American Chemical Society 2012, 134(49), 20117-20130.

[23] Y.Q. Xie, S.D. McAllister, S.A, Hyde, J.P. Sundararajan, B.A. Fouetio-Kengne, D.N. McIlroy, I.F. Cheng. Sulfur as an important co-factor in the formation of multilayer graphene in the thermolyzed asphalt reaction. Journal of Materials Chemistry 2012, 22(12), 5723-5729.

[24] R.S. Nicholson. Theory and Application of Cyclic Voltammetry for Measurement of Electrode Reaction Kinetics. Analytical Chemistry 1965, 37(11), 1351-1355.

[25] S.J. Konopka, B. McDuffie. Diffusion Coefficients of Ferri- and Ferrocyanide Ions in Aqueous Media, Using Twin-Electrode Thin-Layer Electrochemistry. Analytical Chemistry 1970, 42(14), 1741-1746.

[26] P.H. Daum, C.G. Enke. Electrochemical Kinetics of the Ferri-Ferrocyanide Couple on Platinum. Analytical Chemistry 1969, 41(4), 653-656.

[27] M.E.G. Lyons, G.P. Keeley. The Redox Behaviour of Randomly Dispersed Single Walled Carbon Nanotubes both in the Absence and in the Presence of Adsorbed Glucose Oxidase. Sensors 2006, 6, 1791-1826.

[28] C.C.Villarreal, T. Pham, P. Ramnani, A. Mulchandani. Carbon allotropes as sensors for environmental monitoring. Current Opinion in Electrochemistry 2017, 3(1), 106-113.

[29] Kristin K. Cline, Mark T. McDermott, Richard L. McCreery. Anomalously Slow Electron Transfer at Ordered Graphite Electrodes: Influence of Electronic Factors and Reactive Sites. Journal of Physical Chemistry, 1994, 98, 5314-5319.

[30] Richard L. McCreery, Mark T. McDermott. Comment on Electrochemical Kinetics at Ordered Graphite Electrodes. Analytical Chemistry 2012, 84, 2602-2605.

[31] Xiaobo Ji, Craig E. Banks, Alison Crossley, Richard G. Compton. Oxygenated Edge Plane Sites Slow the Electron Transfer of the Ferro-/Ferricyanide Redox Couple at Graphite Electrodes. ChemPhysChem 2006, 7, 1337-1344.

[32] A.N. Patel, M.G. Collignon, M.A. O'Connell, W.O.Y. Hung, K. McKelvey, J.V. Macpherson, P.R. Unwin. A New View of Electrochemistry at Highly Oriented Pyrolytic Graphite. Journal of the American Chemical Society 2012, 134(49), 20117-20130.

[33] Richard L. McCreery. Advanced Carbon Electrode Materials for Molecular Electrochemistry. Chemical Reviews 2008, 108, 2646-2687.

[34] J. Klett, R. Hardy, E. Romine, C. Walls, T. Burchell. High-thermal-conductivity, mesophase-pitch-derived carbon foams: effect of precursor on structure and properties. Carbon 2000, 38, 953-973.

[35] S.H. Kim, G.W. Mulholland, M.R. Zachariah. Density measurement of size selected multiwalled carbon nanotubes by mobility-mass characterization. Carbon 2009, 47, 1297-1302.

[36] J. Robertson. Diamond-like amorphous carbon. Materials science and engineering 2002, R37, 129-281.

[37] L.J. Peng, J.R. Morris. Structure and hydrogen adsorption properties of low density nanoporous carbons from simulations. Carbon 2012, 50(3), 1394-1406.

[38] T. Frauenheim, P. Blaudeck, U. Stephan, G. Jungnickel. Atomic structure and physical properties of amorphous carbon and its hydrogenated analogs. Physical review B 1993, 48(7), 4823-4834.

[39] A. Libassi, A.C. Ferrari, V. Stolojan, B.K. Tanner, J. Robertson, L.M. Brown. Density and sp^3 content in diamond-like carbon films by x-ray reflectivity and electron energy loss spectroscopy. Materials Research Society symposia proceedings 2000, 593, 293-298.

[40] M. Hu, J. He, Z. Zhao, T.A. Strobel, W. Hu, D. Yu, H. Sun, L. Liu, Z. Li, M. Ma, Y. Kono, J. Shu, H. Mao, Y. Fei, G. Shen, Y. Wang, S.J. Juhl, J.Y. Huang, Z. Liu, B. Xu, Y. Tian. Compressed glassy carbon: An ultrastrong and elastic interpenetrating graphene network. Science Advances 2017, 3, e1603213.

[41] D.R. McKenzie. Tetrahedral bonding in amorphous carbon. Reports on Progress in Physics 1996, 59, 1611-1664.

[42] D.A.C. Brownson, M.G. Mingot, C.E. Banks. CVD graphene electrochemistry: biologically relevant molecules. Physical Chemistry Chemical Physics 2011, 13, 20284-20288.

[43] R. Hawaldar, P. Merino, M.R. Correia, I. Bdikin, J. Gracio, J. Mendez, J.A. M. Gago, M.K. Singh. Large-area high-throughput synthesis of monolayer graphene sheet by Hot Filament Thermal Chemical Vapor Deposition. Scientific Reports 2012, 2, 682.

[44] R. John, A. Ashokreddy, C. Vijayan, T. Pradeep. Single- and few-layer graphene growth on stainless steel substrates by direct thermal chemical vapor deposition. Nanotechnology 2011, 22, 165701.

[45] C. Casiraghi, A.C. Ferrari, J. Robertson. Raman spectroscopy of hydrogenated amorphous carbons. Physical Review B 2005, 72, 085401.

[46] R. Blume, D. Rosenthal, J.P. Tessonnier, H. Li, A.K. Gericke, R. Schlogl. Characterizing Graphitic Carbon with X-ray Photoelectron Spectroscopy: A Step-by-Step Approach. ChemCatChem 2015, 7, 2871-2881.

[47] W. Xie, K.M. Ng, L.T. Weng, C.M. Chan. Characterization of hydrogenated graphite powder by X-ray photoelectron spectroscopy and time-of-flight secondary ion mass spectrometry. RSC Advances 2016, 6, 80649-80654.

[48] S.K. Jerng, D.S. Yu, J.H. Lee, C. Kim, S. Yoon, S.H. Chun. Graphitic carbon growth on crystalline and amorphous oxide substrates using molecular beam epitaxy. Nanoscale Research Letters 2011, 6(1), 565.

[49] F. Atchison, T. Bryś, M. Daum, P. Fierlinger, A. Foelske, M. Gupta, R. Henneck, S. Heule, M. Kasprzak, K. Kirch, R. Kötz, M. Kuźniak, T. Lippert, C.F. Meyer, F. Nolting, A. Pichlmaier, D. Schneider, B. Schultrich, P. Siemroth, U. Straumann. Structural characterization of diamond-like carbon films for ultracold neutron applications. Diamond & Related Materials 2007, 16, 334-341.

[50] J.C. Lascovich, R. Giorgi, S. Scaglione. Evaluation of the sp^2/sp^3 ratio in amorphous carbon structure by XPS and XAES. Applied Surface Science 1991, 47, 17-21.

[51] R.J. Yeo. Ultrathin carbon-based overcoats for extremely high density magnetic recording. 2017, ISBN 978-981-10-4881-4.

[52] A. Wollbrink, K. Volgmann, J. Koch, K. Kanthasamy, C. Tegenkamp, Y. Li, H. Richter, S. Kamnitz, F. Steinbach, A. Feldhoff, J. Caro. Amorphous, turbostratic and crystalline carbon membranes with hydrogen selectivity. Carbon 2016, 106, 93-105.

[53] A.M. Dimiev, S. Eigler. Graphene Oxide: Fundamentals and Applications. 2016, ISBN: 978-1-119-06940-9. DOI:10.1002/9781119069447.

[54] A. Ochoa, B. Valle, D.E. Resasco, J. Bilbao, A.G. Gayubo, P. Castano. Temperature Programmed Oxidation Coupled with in situ Techniques Reveal the Nature and Location of Coke Deposited on a Ni/La_2O_3-αAl_2O_3 Catalyst in the Steam Reforming of Bio-oil. ChemCatChem 2018, 10, 2311-2321.

[55] Liangliang Huang, Yuanyuan Cao, Dongfeng Diao. Nanosized graphene sheets induced high electrochemical activity in pure carbon film. Electrochimica Acta 2018, 262, 173-181.

[56] A.C. Ferrari. Determination of bonding in diamond-like carbon by Raman spectroscopy. Diamond and Related Materials 2002, 11, 1053-1061.

[57] Andrea Carlo Ferrari and John Robertson. Raman spectroscopy of amorphous, nanostructured, diamond-like carbon, and nanodiamond. Philosophical Transactions of the Royal Society London A 2004, 362, 2477-2512.

[58] P.M. Wojcik, N. Rajabi, H. Zhu, D. Estrada, P. Davis, K. Livingston, K.M. Yocham, T. Pandhi, I.F. Cheng, D.N. McIlroy. The negative temperature coefficient, electrical resistivity,

and surface morphology of single carbon coated silica nanospring. Materials Chemistry and Physics 2018 (Manuscript Submitted).

[59] B.K. Gupta, Bharat Bhushan. Mechanical and tribological properties of hard carbon coatings for magnetic recording heads. Wear 1995, 190, 110-122.

[60] Aiping Zeng, Victor F. Neto, Jose J. Gracio, Qi Hua Fan. Diamond-like carbon (DLC) films as electrochemical electrodes. Diamond & Related Materials 2014, 43, 12-22.

[61] A. Singha, A. Ghosh, A. Roy, N.R. Ray. Quantitative analysis of hydrogenated diamond like carbon films by visible Raman spectroscopy. Journal of Applied Physics 2006, 100, 044910.

[62] T. Frauenheim, G. Jungnickel, U. Stephan, P. Blaudeck, S. Deutschmann, M. Weiler, S. Sattel, K. Jung, H. Ehrhardt. Atomic-scale structure and electronic properties of highly tetrahedral hydrogenated amorphous carbon. Physical Review B 1994, 50(11), 7940-7945.

[63] Sergey Dub, Petro Lytvyn, Viktor Strelchuk, Andrii Nikolenko, Yurii Stubrov, Igor Petrusha, Takashi Taniguchi, Sergey Ivakhnenko. Vickers Hardness of Diamond and cBN Single Crystals: AFM Approach. Crystals 2017, 7, 369.

[64] R. Jarosova, P.M.D.S. Bezerra, C. Munson, G.M. Swain. Assessment of heterogeneous electron-transfer rate constants for soluble redox analytes at tetrahedral amorphous carbon, boron-doped diamond, and glassy carbon electrodes. Physica Status Solidi A 2016, 213(8), 2087-2098.

[65] S. Chen, Y. Xin, Y. Zhou, F. Zhang, Y. Ma, H. Zhou, L. Qi. Branched CNT@SnO_2 nanorods@carbon hierarchical heterostructures for lithium ion batteries with high reversibility and rate capability. Journal of Materials Chemistry A 2014, 2, 15582-15589.

[66] S.Y. Kim, J. Lee, B.H. Kim, Y.J. Kim, K. S. Yang, M.S. Park. Facile Synthesis of Carbon-Coated Silicon/Graphite Spherical Composites for High-Performance Lithium-Ion Batteries. ACS Applied Materials & Interfaces 2016, 8, 12109-12117.

[67] S.K. Sharma, J. Prakash, P.K. Pujari. Effects of the molecular level dispersion of graphene oxide on the free volume characteristics of poly(vinyl alcohol) and its impact on the thermal and mechanical properties of their nanocomposites. Physical Chemistry Chemical Physics 2015,17, 29201-29209.

[68] F. Cataldo. A study on the thermal stability to 1000°C of various carbon allotropes and carbonaceous matter both under nitrogen and in air. Fullerenes, Nanotubes and carbo nanostructures 2006, 10, 293-311.

[69] X. Li, S. Feng, S. Liu, Z. Li, L. Wang, Z. Zhanand, W. Lu. Fabrication of ZnO nanowires array with nanodiamond as reductant. RSC Advances 2016, 6, 96479-96483.

[70] Y. Kado, T. Goto, R. Hagiwara. Stability of a boron-doped diamond electrode in molten chloride systems. Diamond & Related Materials 2009, 18, 1186-1190.

[71] C. Louro, C.W. Moura, N. Carvalho, M. Stueber, A. Cavaleiro. Thermal stability in oxidative and protective environments of a-C:H cap layer on a functional gradient coating. Diamond & Related Materials 2011, 20, 57-63.

[72] S.G. King, L. McCafferty, V. Stolojan, S.R.P. Silva. Highly aligned arrays of super resilient carbon nanotubes by steam purification. Carbon 2015, 84, 130-137.

[73] S.H. Ng, J. Wang, K. Konstantinov, D. Wexler, J. Chen, H.K. Liu. Spray Pyrolyzed PbO-Carbon Nanocomposites as Anode for Lithium-Ion Batteries. Journal of The Electrochemical Society 2006, 153(4), A787-A793.

[74] Ken Judai, Naoyuki Iguchi, Yoshikiyo Hatakeyama. Low-Temperature Production of Genuinely Amorphous Carbon from Highly Reactive Nanoacetylide Precursors. Journal of Chemistry 2016, 2016, 7840687.

[75] Stanley C. S. Lai, Anisha N. Patel, Kim McKelvey, Patrick R. Unwin. Definitive Evidence for Fast Electron Transfer at Pristine Basal Plane Graphite from High-Resolution Electrochemical Imaging. Angewandte Chemie International Edition 2012, 51, 5405-5408.

[76] M. Fang, K. Wang, H. Lu, Y. Yang, S. Nutt. Covalent polymer functionalization of graphene nanosheets and mechanical properties of composites. Journal of Material Chemistry 2009, 19, 7098-7105.

[77] K. Zhang, Y. Zhang, S. Wang. Enhancing thermoelectric properties of organic composites through hierarchical nanostructures. Scientific Reports 2013, 3, 3448.

[78] B. Andonovic, M. Temkov, A. Ademi, A. Petrovski, A. Grozdanov, P. Paunović, A. Dimitrov. Laue functions model vs scherrer equation in determination of graphene layers number on the ground of XRD data. Journal of Chemical Technology and Metallurgy 2014, 49(6), 545-550.

[79] Tae-Hee Kim, Eun Kyung Jeon, Younghoon Ko, Bo Yun Jang, Byeong-Su Kim, Hyun-Kon Song. Enlarging the d-spacing of graphite and polarizing its surface charge for driving lithium ions fast. Journal of Materials Chemistry A 2014, 2, 7600.

[80] Minzhen Cai, Daniel Thorpe, Douglas H. Adamson, Hannes C. Schniepp. Methods of graphite exfoliation. Journal of Materials Chemistry 2012, 22, 24992-25002.

[81] Kevin W. Hathcock, Jay C. Brumfield, Charles A. Goss, Eugene A. Irene, Royce W. Murray Incipient Electrochemical Oxidation of Highly Oriented Pyrolytic Graphite: Correlation between Surface Blistering and Electrolyte Anion Intercalation. Analytical Chemistry, 1995, 67, 2201-2206.

[82] A.H.R. Palser. Interlayer interactions in graphite and carbon nanotubes. Physical Chemistry Chemical Physics 1999, 1, 4459-4464.

[83] K. Spyrou, P. Rudolf. An Introduction to Graphene: Functionalization of Graphene. Wiley-VCH Verlag GmbH & Co. KGaA. 2014, ISBN: 9783527672790.

[84] Yun Wu, Takeyoshi Okajima, Takeo Ohsaka. Lithium Intercalation into Graphene Ribbons of Glassy Carbon. International Journal of Electrochemical Science 2017, 12, 1004-1013.

[85] Meng Hu, Julong He, Zhisheng Zhao, Timothy A. Strobel, Wentao Hu, Dongli Yu, Hao Sun,1 Lingyu Liu, Zihe Li, Mengdong Ma, Yoshio Kono, Jinfu Shu, Ho-kwang Mao, Yingwei Fei, Guoyin Shen, Yanbin Wang, Stephen J. Juhl, Jian Yu Huang, Zhongyuan Liu, Bo Xu, Yongjun Tian. Compressed glassy carbon: An ultrastrong and elastic interpenetrating graphene network. Science Advances 2017, 3, e1603213.

[86] O.V. Kharissova, B. I. Kharisov. Variations of interlayer spacing in carbon nanotubes. RSC Advances 2014, 4, 30807-30815.

[87] K.B. Teo, C. Singh, M. Chhowalla, W.I. Milne. Catalytic Synthesis of Carbon Nanotubes and Nanofibers. Encyclopedia of Nanoscience and Nanotechnology. American Scientific Publisher 2003, X, 1–22.

[88] R. Bajpai, L. Rapoport, K. Amsalem, H.D. Wagner. Rapid growth of onion-like carbon nanospheres in a microwave oven. CrystEngComm 2016, 18, 230-239.

[89] B. Manoj, A.G. Kunjomana. Study of Stacking Structure of Amorphous Carbon by X-Ray Diffraction Technique. International Journal of Electrochemical Science 2012, 7, 3127-3134.

[90] L.M. Malard, M.A. Pimenta, G. Dresselhaus, M.S. Dresselhaus. Raman spectroscopy in graphene. Physics Reports 2009, 473, 51-87.

[91] Y. Hishiyama, M.Nakamura. X-ray diffraction in oriented carbon films with turbostratic structure. Carbon 1995, 33, 1399-1403.

[92] C.J. Thambiliyagodage, S. Ulrich, P.T. Araujo, M.G. Bakker. Catalytic graphitization in nanocast carbon monoliths by iron, cobalt and nickel nanoparticles. Carbon 2018, 134, 452-463.

[93] A. Vuong, T. Trevethan, C.D. Latham, C.P. Ewels, D. Erbahar, P.R. Briddon, M.J. Rayson, M.I. Heggie. Interlayer vacancy defects in AA-stacked bilayer graphene: density functional theory predictionsJournal of Physics: Condensed Matter 2017, 29, 155304.

[94] M. Yoon, J. Howe, G. Tibbetts, G. Eres, Z. Zhang. Polygonization and anomalous graphene interlayer spacing of multi-walled carbon nanofibers. Physical Review B 2007, 75, 165402.

[95] E.A. Belenkov. Formation of Graphite Structure in Carbon Crystallites. Inorganic Materials 2001, 37(9), 928-934.

[96] T. Watanabe, T.K. Shimizu, Y. Tateyama, Y. Kim, M. Kawai, Y. Einaga. Giant electric double-layer capacitance of heavily boron-doped diamond electrode. Diamond & Related Materials 2010, 19, 772-777.

[97] H. Naragino, K. Yoshinaga, A. Nakahara, S. Tanaka, K. Honda. Enhancement of electrical conductivity and electrochemical activity of hydrogenated amorphous carbon by incorporating boron atoms. Journal of Physical Chemistry Conference Series 2013, 441, 12042.

[98] Q. Xue, D. Kato, T. Kamata, S. Umemura, S. Hirono, O. Niwa, Electron Cyclotron Resonance-Sputtered Nanocarbon Film Electrode Compared with Diamond-Like Carbon and Glassy Carbon Electrodes as regards Electrochemical Properties and Biomolecule Adsorption. Japanese Journal of Applied Physics 2012, 51, 90124.

[99] K.S. Yoo, B. Miller, R. Kalish, X. Shi. Electrodes of nitrogen-incorporated tetrahedral amorphous carbon - A novel thin-film electrocatalytic material with diamond-like stability. Electrochemical and Solid State Letters 1999, 5, 233-235.

[100] A.P. Zeng, M.M. Bilek, D.R. McKenzie, P.A. Lay, A. L. Fontaine, V.J. Keast. Correlation between film structures and potential limits for hydrogen and oxygen evolutions at a-C:N film electrochemical electrodes. Carbon 2008, 46(4), 663-670.

[101] W. Wang, Z. Wei, W. Su, X. Fan, J. Liu, C. Yan, C. Zeng. Kinetic investigation of vanadium (V)/(IV) redox couple on electrochemically oxidized graphite electrodes. Electrochimica Acta 2016, 205, 102-112.

[102] B. Caglar, J. Richards, P. Fischer, J. Tuebke. Conductive polymer composites and coated metals as alternative bipolar plate materials for all-vanadium redox-flow batteries. Advanced Materials Letters 2014, 5(6) 299-308.

[103] W.L. Wang, S.M. Heb, C.H. Lan. Protective graphite coating on metallic bipolar plates for PEMFC applications. Electrochimica Acta 2012, 62(15), 30-35.

[104] S. Viswanathan, L. Mohan, P. Bera, V. P. Kumar, Harish C. Barshilia, C. Anandan. Corrosion and Wear Behaviors of Cr-Doped Diamond-Like Carbon Coatings. Journal of Materials Engineering and Performance 2017, 26(8), 3633-3647.

[105] Mingjun Cui, Jibin Pu, Jun Liang, Liping Wang, Guangan Zhang, Qunji Xue. Corrosion and tribocorrosion performance of multilayer diamond-like carbon film in NaCl solution. RSC Advances 2015, 5, 104829-104840.

[106] J. Bautista-Ruiz, J.C. Caicedo, W. Aperador. Tribocorrosion Behavior of Amorphous Carbon-Silicon Coated Titanium in Biological Medium. Tribology in Industry 2018, 40(2), 326-334.

[107] M. Madej, D. Ozimina, K. Kurzydlowski, T. Plocinski, P. Wiecinski, P. Baranowicz. Diamond-like carbon coatings in biotribological applications. Kovove Materialy 2016, 54(3), 185-194.

[108] R.K. Das, Y. Wang, S.V. Vasilyeva, E. Donoghue, I. Pucher, G. Kamenov, H.P. Cheng, A.G. Rinzler. Extraordinary Hydrogen Evolution and Oxidation Reaction Activity from Carbon Nanotubes and Graphitic Carbons. ACS Nano 2014, 8(8), 8447-8456.

[109] M.C. Oliveira, A.S. Viana, A.M.B. Rego, A.M. Ferraria, P.B. Tavares, A.D. Veloso, R.A. Videira. Dual Behaviour of Amorphous Carbon Released Electrochemically from Graphite. ChemistrySelect 2016, 1, 4126-4130.

[110] Xingyi Yang, Lars Haubold, Gabriel DeVivo, Greg M. Swain. Electroanalytical Performance of Nitrogen-Containing Tetrahedral Amorphous Carbon Thin-Film Electrodes. Analytical Chemistry 2012, 84, 6240-6248.

[111] Tomoyuki Kamata, Dai Kato, Hideo Ida, Osamu Niwa. Structure and electrochemical characterization of carbon films formed by unbalanced magnetron (UBM) sputtering method. Diamond & Related Materials 2014, 49, 25-32.

[112] Tomoyuki Kamata, Dai Kato, Shigeru Hirono, Osamu Niwa. Structure and Electrochemical Performance of Nitrogen-Doped Carbon Film Formed by Electron Cyclotron Resonance Sputtering. Analytical Chemistry 2013, 85, 9845-9851.

[113] Daniel Bousa, Jan Luxa, David Sedmidubsky, Stepan Huber, Ondrej Jankovsky, Martin Pumera, Zdenek Sofer. Nanosized graphane $(C_1H_{1.14})_n$ by hydrogenation of carbon nanofibers by Birch reduction method. RSC Advances 2016, 6, 6475-6485.

[114] Jun Li, Alan Cassell, Lance Delzeit, Jie Han, M. Meyyappan. Novel Three-Dimensional Electrodes: Electrochemical Properties of Carbon Nanotube Ensembles. Journal of Physical Chemistry B 2002, 106, 9299-9305.

[115] Ryan R. Moore, Craig E. Banks, Richard G. Compton. Basal Plane Pyrolytic Graphite Modified Electrodes: Comparison of Carbon Nanotubes and Graphite Powder as Electrocatalysts. Analytical Chemistry 2004, 76, 2677-2682.

[116] Irene Taurino, Sandro Carrara, Mauro Giorcelli, Alberto Tagliaferro, Giovanni De Micheli. Comparison of two different carbon nanotube-based surfaces with respect to potassium ferricyanide electrochemistry. Surface Science 2012, 606, 156-160.

Supplementary Information

The sp^2-sp^3 Carbon Hybridization Content of Nanocrystalline Graphite from Pyrolyzed Vegetable Oil, Comparison of Electrochemistry and Physical Properties with Other Carbon Forms and Allotropes.

Humayun Kabir[1], Haoyu Zhu[1], Jeremy May[1], Kailash Hamal[1], Yuwei Kan[1], Thomas Williams[2], Elena Echeverria[3], David N. McIlroy[3], David Estrada[4], Paul H. Davis[4], Twinkle Pandhi[4], Katie Yocham[4], Kari Higginbotham[4], Abraham Clearfield[5], I. Francis Cheng[1,*]

[1] Department of Chemistry, University of Idaho, 875 Perimeter Dr, MS 2343, Moscow, ID 83844, USA

[2] Department of Geological Sciences, University of Idaho, 875 Perimeter Dr, MS 3022, Moscow, ID 83844, USA

[3] Department of Physics, Oklahoma State University, 145 Physical Sciences Building, Stillwater, OK 74028, USA

[4] Micron School of Materials Science and Engineering, Boise State University, 1910 University Drive, Boise, ID 83725, USA

[5] Department of Chemistry, Texas A&M University, College Station, TX 77843, USA

*Corresponding author: Tel: (208) 885-6387, E-mail: ifcheng@uidaho.edu (I. Francis Cheng)

Scanning Electron Micrographs (SEM) of GUITAR and Highly Ordered Pyrolytic Graphite (HOPG)

In addition to Figure 2 (presented in the manuscript), Figure S1 shows more SEM images of GUITAR (A, B and C) and highly ordered pyrolytic graphite (HOPG) (D, E and F), in order to better understand their morphological similarities and differences. Both GUITAR and HOPG show clear basal and edge plane configurations. However, in contrast to HOPG, GUITAR does not show any step defects. Figure S1A shows defect free basal plane of GUITAR at an accelerating voltage of 5 kV. GUITAR's basal plane appeared flat and featureless to the resolution of SEM.

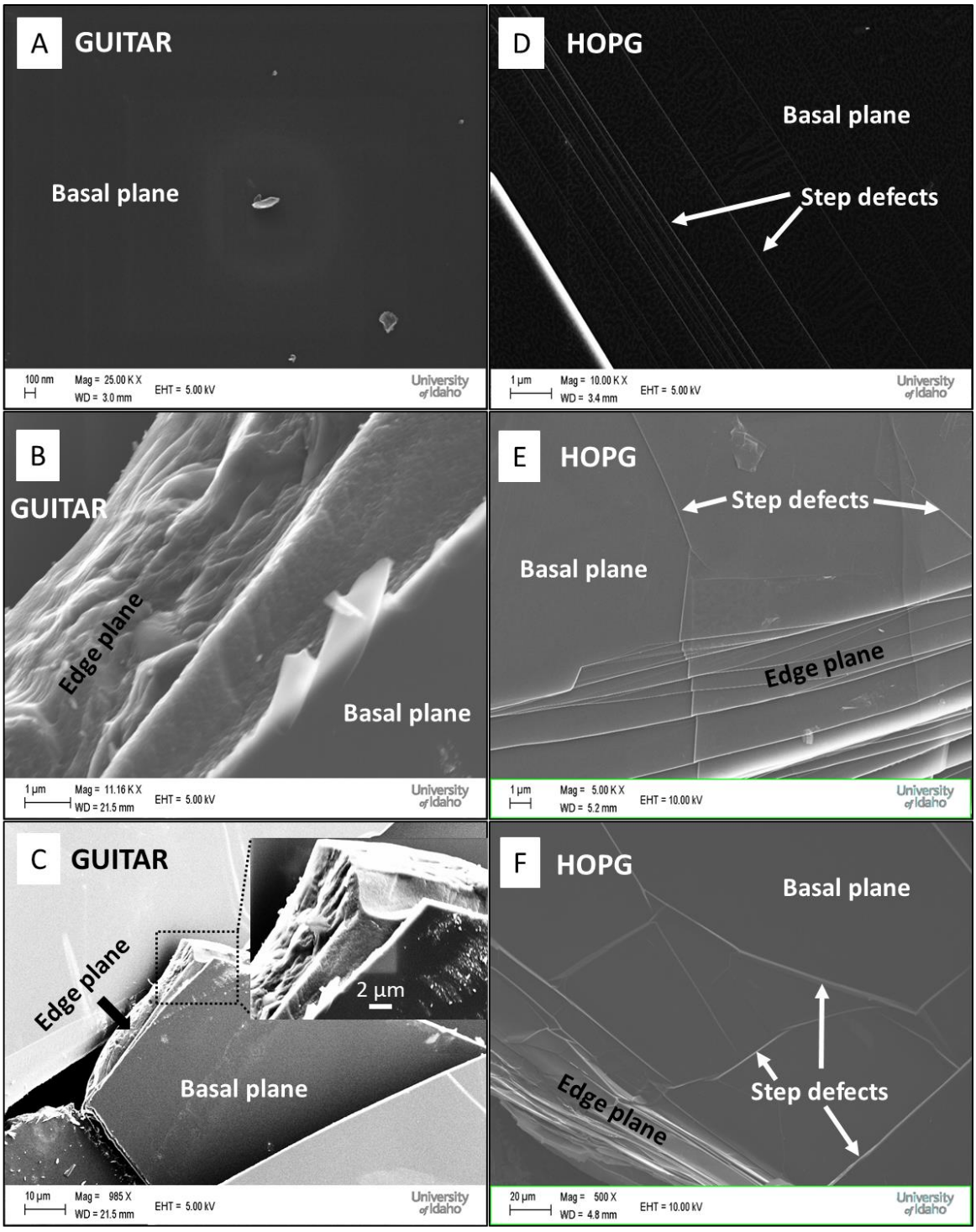

Figure S1. Scanning electron micrographs of GUITAR (A, B and C) and HOPG (D, E and F). Both show clear basal and edge plane configurations. In contrast to HOPG, GUITAR does not show any step defects. HOPG is found to have a mean step density of 0.5 µm/µm^2, as calculated in this study as well as reported by Unwin et al (Ref. 21 in the manuscript).

Electrochemical Properties of GUITAR

Cyclic voltammograms on BP-GUITAR at 50 mV/s in a solution of 1 mM $Fe(CN)_6^{3-}$ in 1 M KCl and 1 M H_2SO_4 are shown in Figure S2. Figure S2A shows the difference between the cathodic and anodic peak potentials in 1 mM $Fe(CN)_6^{3-}$ is 65 mV. This corresponds to a standard HET rate constant (k^0) of 0.03 cm/s, calculated from the Nicholson method and verified by modelling experimental cyclic voltammograms using BASi DigiSim software. Figure S2B shows that GUITAR's total electrochemical potential window is 3 V in 1 M H_2SO_4 at 200 µA/cm^2, with anodic limit 1.9 V (vs. Ag/AgCl) and the cathodic limit -1.1 V (vs. Ag/AgCl).

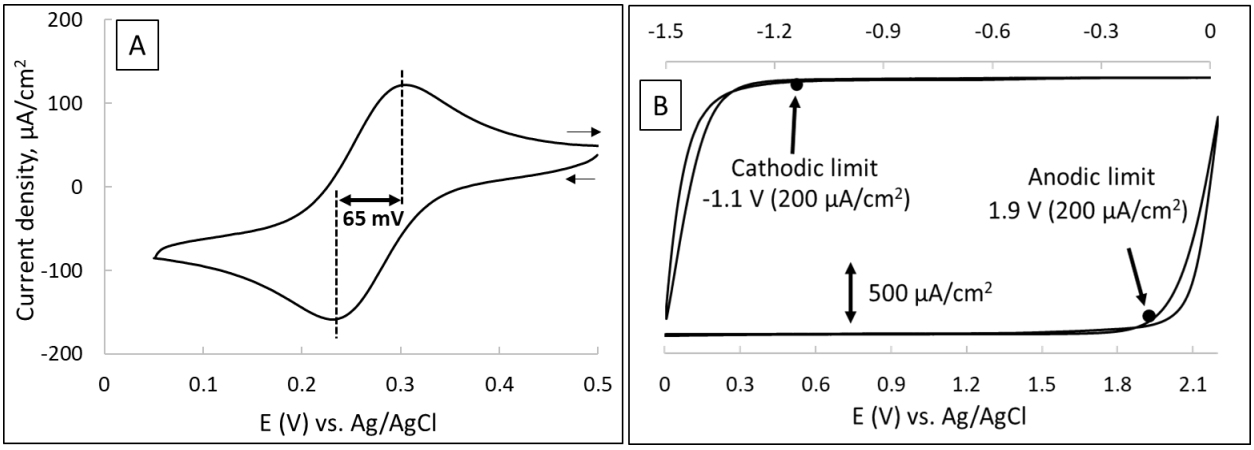

Figure S2. Cyclic voltammograms on BP-GUITAR at 50 mV/s in A) 1 mM $Fe(CN)_6^{3-}$ (in 1 M KCl) and B) 1 M H_2SO_4. Figure S2A indicates a HET rate constant (k^0) of 0.03 cm/s, and S2B indicates a total potential window of 3 V at 200 µA/cm^2.